C. R. Mecanique 344 (2016) 195–207

Contents lists available at ScienceDirect

Comptes Rendus Mecanique

www.sciencedirect.com

# The inertial power and inertial force of robotic and natural bat wing

Dongfu Yin *, Zhisheng Zhang

*School of Mechanical Engineering, Southeast University, Nanjing, Jiangsu, 211189, China*

ARTICLE INFO

*Article history:*
Received 12 July 2015
Accepted 9 November 2015
Available online 3 February 2016

*Keywords:*
Inertial power
Inertial force
Bat wing
Skeleton
Robotic bat
Computational model

ABSTRACT

Based on the acquired length and angle data of bat skeletons, a four-degree freedom robotic bat wing and an identical computational model with flap, sweep, elbow and wrist motions were presented. By considering the digits motions, a biomimetic bat skeleton model with seven-degree freedom was established as well. The effects of frequency, amplitude and downstroke ratio, as well as the components of inertial power and force on different directions, were studied. The experimental and computational results indicated that the inertial power and force accounted for the largest part on flap direction, the wing fold during upstroke could reduce the inertial power and force.



## 1. Introduction

Bats have heavy muscular wings with joints that enable higher degrees of dexterity [1]. For different bat species, although the wing mass account for only 11% to 20% of the total bat mass [2], it generates enough lift and thrust to maintain bat flying. The distinctive capacity for powered flight subjects the limb skeletons of bats [3]. The skeletons are important constitutive parts of the wing. They are used to support the wing membrane to generate lift and thrust, to resist primarily bending forces and large torsional forces, to withstand the loads applied to them, and to achieve complex movements by changing the angles between different bones.

The inertial power and force are the power and force needed to make the wings oscillate [4]. Unlike fixed-wing aircrafts, flying organisms cannot continuously generate constant lift and thrust [2]. In each flap cycle, the wing has two accelerations and two decelerations, and the inertial power and force will be changed along with the change of velocities and accelerations. Although the inertial power of native bat wing has already been studied [2,5,6], these results often include the effects of wing membrane, and the effects of the skeleton on the inertial power and force require further investigation.

A flying bat must do work with its flight muscles to move the wings; the rate at which this work is done is the mechanical power [4]. The ratio of inertial power to mechanical power remains controversial [4–9]. Although the inertial power might account for a small percentage of the total power for some native bats [10], this may not be applicable for the robotic bat. By analyzing the recently designed and fabricated robotic bat wings, we found that it is different from the native thinner skeletons; the robotic bat skeletons were often strengthened by increasing the size or selecting high-density materials to keep the rigidity [11–15]. Therefore, for the robotic bat wing, the inertial power and force might be larger than the actual bat skeletons and cannot be neglected.

* Corresponding author. Tel.: +86 15205181132.
*E-mail address:* ydf678@hotmail.com (D. Yin).

http://dx.doi.org/10.1016/j.crme.2015.11.002
1631-0721/

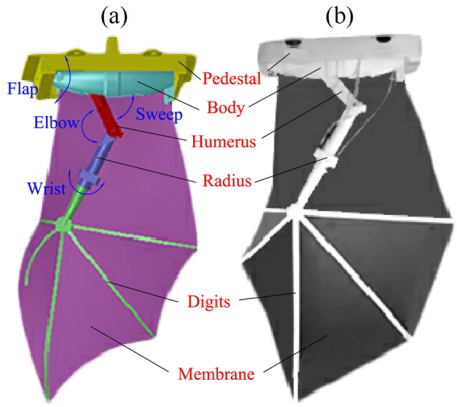


**Fig. 1.** The motions and structure of the robotic bat wing. (a) Solid works model. (b) Fabricated model.

The inertia force is also an important factor that needs to be considered for the future robotic bat wing design, especially for the large-scaled models. Some simple theoretical formulas of flap motion have been proposed to investigate the factors that affect the inertial power [6,16], but not enough attention has been paid on the effects of inertial force. Meanwhile, some parameters, such as the frequency, amplitude, downstroke ratio, etc., which affect the flight efficiency remarkably might have obvious influence on the robotic bat wing as well. How these factors affect the inertia power and force on bat skeletons still needs to be revealed. As a result, models or equations that can reflect the relationships between the above parameters and inertial power and force need to be established.

For the robotic bat wing, multiple motors were combined to realize complicated manoeuvres of the wing [12–15]. But for a particular motor, it can only change one motion direction. The flap, sweep and elbow motions were three major movements that accounted for the largest proportion of inertial power [13], and these three motions correspond to the inertial power on up–down, forward–backward and expand–contract directions. On the other hand, the robotic wing was installed on the test section and the instantaneous inertial forces quantified with load cells [12–15]. For a full-motion bat wing, it imposes inertial force on the lift direction, the drag direction, and the spanwise direction. The analysis of inertial power and force on different directions can help to choose appropriate motors and load cells for future robotic bat design and application.

In the present study, the influence of bat skeleton movements on inertial power and force were studied. Based on the size and real-time angle data of *Eptesicus fuscus*, a 4DOF (four degrees of freedom) robotic bat wing was designed and fabricated (Fig. 1). Uniformly, a same 4DOF bat skeleton computational model with divided fragments was established to compare the inertial values with the robotic bat wing. Appended with the digit motions, the 4DOF model was then extended to a more accurate 7DOF (seven degrees of freedom) calculation model. Combined with the 4DOF computational model, the sinusoidal flap theoretical equations were detailed to indicate the impact factors to the inertial power and force. The influence of frequency, amplitude, downstroke ratio on the inertial power and inertial force of the 4DOF robotic bat wing, 4DOF and 7DOF computational models were compared together. The inertial power and force components on up–down, stretch–shrink, and fore–aft directions of different fragments were also studied.

## 2. Materials and methods

### 2.1. Robotic bat wing

For a bat in level flight, the right wing was used to define the coordinate system. The positive $X$ direction was along the bat tail to head, the positive $Y$ direction was along the wing root to wingtip, the positive $Z$ direction was perpendicular to the $XY$ plane and pointing up. Seven angles were used to describe the complex movements between different skeletons of the bat's wing. These angles reflect the bat wing's flap motion, stretch-shrink motion, rotate motion and motions between digits. For a horizontal flight bat, the flap angle was defined as the angle between the humerus and the horizontal plane. The sweep angle was defined as the angle between the humerus and the vertical plane. The elbow angle was calculated as that between the humerus and the radius. The wrist angle was the angle between two planes, one plane was composed by shoulder joint, elbow joint and wrist joint, another plane consisted of wrist joint, digit3 and digit5 tip markers. Three radius-digit angles were defined as the angle between the radius and the corresponding digit. Nontoxic markers were drawn on the joints and tips of the bat wing, and high-speed cameras (Photron Fastcam-X 1280 PCI camera) were used to track the marker positions during the bat's flight. The real-time angles were calculated based on the obtained marker positions. Fig. 2 shows the real-time angle changing curves of a typical bat.

Based on the measured bat skeleton length and angle data, a 4DOF robotic bat skeleton model was established in Solidworks software and manufactured by a 3D printer (Dimension 1200es, Stratasys). The robotic bat wing was composed by pedestal, body, humerus, radius and digits. To reduce the number of motors and the complexity of the model, the

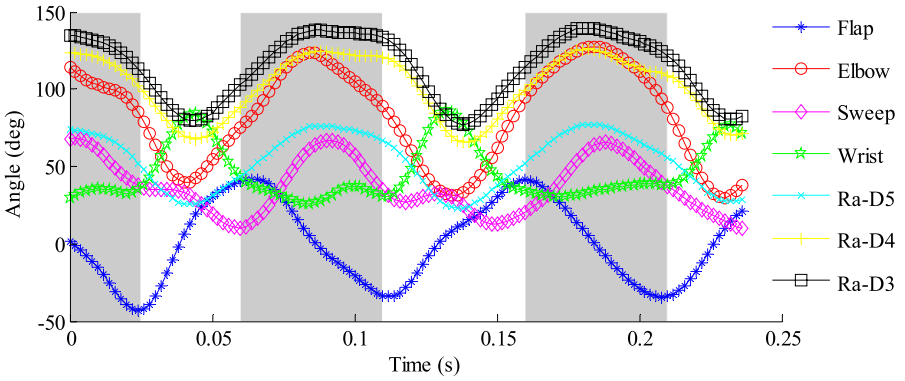


**Fig. 2.** Real-time angle curves of a typical bat. Ra-D5, Ra-D4, Ra-D3 represent the angles between radius and digit5, digit4, digit3, respectively.

movements of the digits were not added in this model (Fig. 1). The material of the skeletons was ABS and the size of robotic wing was scaled two times as native bat wing. Because the material we used to make skeletons does not have enough rigidity and flexibility as native bat bones, the robotic bat wing was scaled larger to strengthen the rigidity and avoid breakdown. The geometric, kinematic and dynamic similarities were considered when the robotic wing was scaled. As we mainly considered the relationship between power, force and some flight parameters in this paper, for a specific robotic bat wing, the scaled size has little influence over the regulations between these factors.

The accurate motions were respectively powered by four motors (BE163CJ-NFON, Parker Compumotor) and controlled by a DMC controller (DMC-4060, Galil Motion Control); the trajectory of each motion was followed by the bat angle data we got. Steel wires, plastic hollow tubes and metal pins were used to connect different bones and transmit movements from motors to bat wing.

The robotic bat wing was fixed on the test section and mounted on top of the wind tunnel. Lift and drag were measured by two cross vertical distributed load cells, and power was calculated as the product of motor torque and velocity. The load cells were calibrated and validated, the force and power data were fitted and a variety of error factors were considered to eliminate or reduce the errors. The required frequency, amplitude and downstroke ratio were achieved by controlling the motor rotation speed and the amplitude in a cycle. The initial position of the robotic bat wing was selected at the middle downstroke position. At that moment, the flap angle was 0, the wrist angle was close to the minimum and other five angles approximated to the maximum. Sequentially, the flight motion was divided into four phases in this paper, downward deceleration, upwards acceleration, upwards deceleration, and downward acceleration phase [13,15,18,19].

### 2.2. Computational model of bat wing skeletons

Based on the flap angle data (Fig. 2) and other simplified models to calculate the inertial power of bats [7], the flap motion can be simplified to a sinusoidal movement when small deviations are not considered. For a rigid wing, the transient flap angle $r(t)$, the transient angular velocity $\mathrm{d}r/\mathrm{d}t$, and the transient angular acceleration $\mathrm{d}^2r/\mathrm{d}t^2$ can be described by the following equation:

$$\begin{aligned} r(t) &= \frac{1}{2}\varphi \sin(2\pi f t) + \varphi_0 \\ \frac{\mathrm{d}r}{\mathrm{d}t} &= \pi f \varphi \cos(2\pi f t) \\ \frac{\mathrm{d}^2 r}{\mathrm{d}t^2} &= -2\pi^2 f^2 \varphi \sin(2\pi f t) \end{aligned} \tag{1}$$

where $\varphi$ is the amplitude, $\varphi_0$ is the initial amplitude, $f$ is the frequency. The inertial energy $E(t)$ and inertial power $P$ of sinusoidal flap during a complete wingbeat cycle can be calculated as:

$$\begin{aligned} E(t) &= \int \left( I \times \frac{\mathrm{d}r}{\mathrm{d}t} \times \frac{\mathrm{d}^2 r}{\mathrm{d}t^2} \right) \mathrm{d}t = -\int I\pi^3 f^3 \varphi^2 \sin(4\pi f t)\mathrm{d}t = \frac{1}{4} I\pi^2 f^2 \varphi^2 \cos(4\pi f t) + C \\ P &= -4 \int_0^{\frac{1}{4f}} I\pi^3 f^4 \varphi^2 \sin(4\pi f t)\mathrm{d}t = I\pi^2 f^3 \varphi^2 \end{aligned} \tag{2}$$

where $C$ is the integration constant, $I$ is the moment of inertia. The values of inertial energy and power are in accordance with D.K. Riskin's results [6], but account for half of C. Vandenberg's ones [7]. These differences might lie in different

approaches dealing with the negative power. The instantaneous inertial power is positive at the acceleration stage, but negative at the deceleration stage. Whether the negative power can be stored or converted into useful aerodynamic work that occurs during wing deceleration was still controversial, and these controversial results lead to a one to two times difference in the total power [6,7]. Unlike the native flight animals, the motors that are used to measure the power have no devices, such as elastic elements, to store the negative energy and convert it into useful work during the acceleration stage. So only the positive work for two acceleration phases of one wing beat was considered, and the inertial power was calculated by multiplying the positive work by the wing beat frequency. In accordance with the experimental settings, the negative power was also neglected in the computational models. While frequency, amplitude and downstroke ratio to the inertial power and force were mainly considered in the present study, this assumption would not affect the variation tendencies.

The inertial force can be calculated as the product of mass $m$ and linear acceleration $a$. The total inertial force of the wing is the superposition of three orthogonal components. Analogously, when flap movement of rigid wing simplified to a simple harmonic motion, the linear displacement $s(t)$, the linear acceleration $\mathrm{d}^2s/\mathrm{d}t^2$ and the inertial force $F$ of each component can be expressed as

$$\begin{aligned} s(t) &= \frac{1}{2}x\sin(2\pi ft) + x_0 \\ \frac{\mathrm{d}^2s}{\mathrm{d}t^2} &= -2\pi^2 f^2 x\sin(2\pi ft) \\ F &= -2m\pi^2 f^2 x\sin(2\pi ft) \end{aligned} \tag{3}$$

where $x$ is the maximum displacement and $x_0$ is the initial displacement. Note that, for any point of the rigid bat wing skeleton of flap motion, it only has the movements on up-down ($Z$) direction and stretch-contract ($Y$) direction. The total inertial power and inertial force result from the superposition of these two components. In this respect, the wing has only two-dimensional motions in a plane. But when sweep, elbow, wrist motions and movements among digits are considered, the wing has a complex three-dimensional movement in space, and the above simplified models are not applicable in this case. To achieve accurate results, the bat wing skeleton was divided into small fragments. The inertial energy and force were first calculated for each small part, and then accumulated to get the overall results of the bat wing skeletons. The inertial power is the sum of all positive changes in inertial energy over the course of the wingbeat cycle multiplied by the wingbeat frequency. The inertial energy $E$, the inertial power $P$ and inertial force $F$ of the bat wing skeleton are as follows:

$$\begin{aligned} E &= \frac{1}{2}\sum_{n=1}^{k} m_n v_n^2 \\ P &= Ef = \frac{1}{2}f\sum_{n=1}^{k} m_n v_n^2 \\ F &= ma = \sum_{n=1}^{k} m_n a_n \end{aligned} \tag{4}$$

where $n$ is the $n$th segment, $k$ is the total number of segments, $a$ is the synthetic acceleration and $v$ is the relative velocity of the segment to the shoulder.

As the velocity and acceleration are varying at different positions on the wing, it is not accurate to calculate the inertial power and force by using the wing centroid velocity and acceleration. In another previous model, the wing was divided into small segments to calculate the inertial power and force separately, and the separate results were summed to calculate the total values [5]. However, these segments were mainly cut to the long rectangular shape, and the masses, velocities and accelerations were calculated based on rectangular strips [5]. Because of the complexity of the bat wing's movements, the rectangle strips might have the fold and twist of locomotion. And the velocities and accelerations would be different at the two sides, so the centroid velocity and acceleration could not accurately represent the real values of the corresponding strip. In our computational model, the wing skeletons were divided into small segments directly (Fig. 3 and Fig. 4); each part had no definite shape and the mass distributions along the bone nearly constant with respect to digit, radius, humerus and body part (Table 1 and Table 2). Due to the rigid connection and small size of the segments, the fold and twist effect can be neglected.

A computational model with the same size and mass properties as our robotic bat wing was presented to calculate inertial power and force. As the pedestal part did not move during the simulation, only the effects of the other four parts, including digits, radius, humerus, and body, were analyzed. Although the mass of the digits is small, they might have more complicated motions and higher velocities and accelerations. To get accurate results, the digits were divided into more segments than the other three parts. The skeletons were divided into 35 fragments in total to ensure the accuracy of calculations (see appendix). The Adams software was used to simulate the bat wing's motions. The size, material, forms of motion, direction of motion, degrees of freedom, and initial position of the model were defined or set the same as the

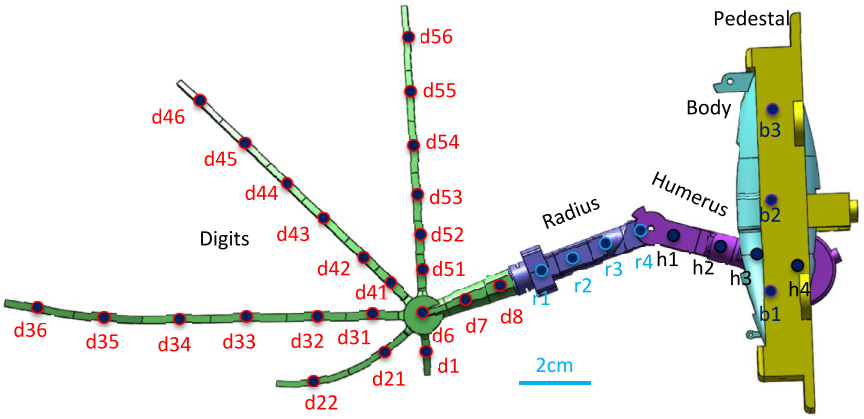


**Fig. 3.** The fragments and the mass distribution of the 4DOF robotic bat wing skeleton. The solid circles refer to the mass center of small fragments, with different edge colors refers to different parts of the robotic bat wing skeleton. The digit, radius, humerus and body parts were divided to 24 (d1–d8), 4 (r1–r4), 4 (h1–h4) and 3 (b1–b3) fragments respectively, with 35 fragments in total.

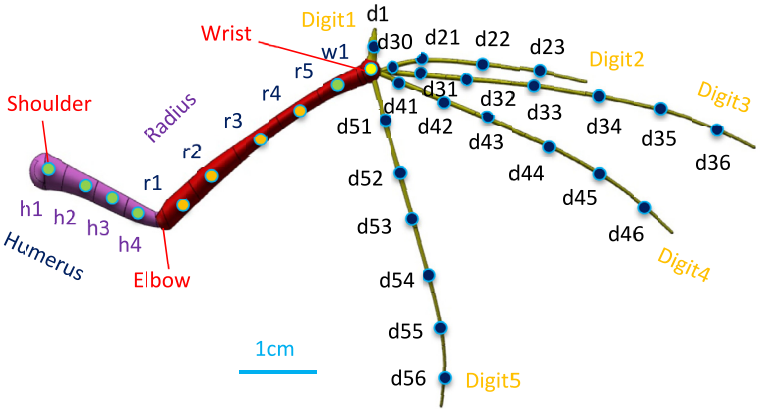


**Fig. 4.** The fragments and mass distribution model of the 7DOF bat wing. The solid circles refer to the mass center of small fragments, while different filled colors refer to different parts of the robotic bat wing skeleton. The humerus, radius, wrist, digit1, digit2, digit3, digit4 and digit5 were divided into 4 (h1–h4), 5 (r1–r5), 1 (w1), 1 (d1), 3 (d21–d23), 7 (d30–d36), 6 (d41–d46) and 6 (d51–d56) fragments respectively, with 33 fragments in total.

**Table 1**
Mass distribution of the 4DOF bat wing skeleton model.

| Mark | Mass (g) | Mark | Mass (g) | Mark | Mass (g) | Mark | Mass (g) | Mark | Mass (g) |
|---|---|---|---|---|---|---|---|---|---|
| d1 | 0.054 | d35 | 0.154 | d46 | 0.074 | d6 | 1.032 | h1 | 1.738 |
| d21 | 0.155 | d36 | 0.157 | d51 | 0.089 | d7 | 0.730 | h2 | 1.086 |
| d22 | 0.126 | d41 | 0.084 | d52 | 0.083 | d8 | 0.905 | h3 | 0.816 |
| d31 | 0.117 | d42 | 0.078 | d53 | 0.116 | r1 | 1.581 | h4 | 5.090 |
| d32 | 0.129 | d43 | 0.103 | d54 | 0.118 | r2 | 1.049 | b1 | 7.474 |
| d33 | 0.169 | d44 | 0.080 | d55 | 0.110 | r3 | 0.971 | b2 | 16.222 |
| d34 | 0.155 | d45 | 0.094 | d56 | 0.128 | r4 | 0.771 | b3 | 13.858 |

**Table 2**
Mass distribution of the 7DOF bat wing skeleton model.

| Mark | Mass (mg) | Mark | Mass (mg) | Mark | Mass (mg) |
|---|---|---|---|---|---|
| h1 | 263.96 | d21 | 7.85 | d42 | 7.96 |
| h2 | 185.58 | d22 | 6.20 | d43 | 6.43 |
| h3 | 127.32 | d23 | 4.15 | d44 | 5.64 |
| h4 | 84.615 | d30 | 5.38 | d45 | 4.71 |
| r1 | 203.97 | d31 | 7.96 | d46 | 2.60 |
| r2 | 213.90 | d32 | 9.06 | d51 | 7.43 |
| r3 | 146.91 | d33 | 8.55 | d52 | 7.49 |
| r4 | 109.53 | d34 | 5.74 | d53 | 5.64 |
| r5 | 115.15 | d35 | 4.12 | d54 | 5.76 |
| w1 | 62.45 | d36 | 2.46 | d55 | 3.73 |
| d1 | 14.64 | d41 | 8.30 | d56 | 3.22 |

experimental robotic bat wing. The continuous velocities and accelerations of each fragment within a wingbeat cycle were calculated automatically by the software. And these data were exported to Matlab software to calculate the inertial power and force of the separated fragments and the total bat skeleton.

Due to the manufacture, assemblage and rigidity requirements, the size of the robotic bat wing was two times that of the native bat. Some parts such as the digits were also strengthened to ensure the rigidity, and only four main motions were used to imitate the wing movements. Therefore, the robotic bat wing and the 4DOF model have some differences with the native bat wing. To develop a discrete mass system that can represent the bat wing more accurately, a 7DOF bat skeleton model was established. The lengths and diameters of one bat wing skeletons, including the taper digits, were measured in detail. Then the three-dimensional bat wing skeleton model was set up in Solidworks software. Compared with the 4DOF model, three more degrees of freedom were added to simulate the digits motions. The angle changes between radius and digit3, radius and digit4, radius and digit5 were newly added. The distal radius was separated as a wrist joint part, which has a rotary motion perpendicular to the radius. Because digit1, digit2 and digit3 had similar movements during bat flight, the angle changes between digit1 and radius, digit2 and radius were set the same as digit3 and radius, and these three digits were fixed as one part in the simulation model. A constant density was set to the bones at 2000 kg/m$^3$ based on typical values for compact cortical bone in mammals [2]. For a single bat wing, the mass of skeletons in our model was 1.6 g. Compared with the native bat *Eptesicus fuscus*, it took about 5% to 11% of the total mass of the bat [20]. In one flight cycle, 50 equidistant spacing points from each bat angle changing data were used to mimic the real bat angle curves (Fig. 2). These data were fitted to seven smooth paths for that the corresponding skeleton followed by. The initial location of the model was set at the middle downstroke position. At this moment, the flap angle and the wrist angle were apparently at the minimum values, while other five angles at their maximum values.

## 3. Results

### 3.1. The effects of frequency, amplitude and downstroke ratio

Frequency, amplitude and downstroke ratio ($\tau$) are three main factors that affect the inertial power and inertial force. The downstroke ratio is defined as the downstroke fraction of one wingbeat cycle [21]. In consideration of the native bats' parameters range and the bearing capacity of our robotic bat wing, the frequency, amplitude and downstroke ratio scope of the experiment and of the computation were set as 0.5 to 5 Hz, 18 to 144° and 0.35 to 0.65, respectively. The default values of these three parameters were 3 Hz, 126° and 0.5. When one parameter was studied, the other two were kept constant. The inertial force at different directions was considered separately. It was decomposed to inertial lift ($F_{\mathrm{L}}$) on the $Z$ axis and inertial drag ($F_{\mathrm{D}}$) on the $X$ axis. The total experimental errors, including system errors and random errors, were basically constant. The maximum absolute errors of power and force were less than 0.1 W and 0.1 N severally. Except for the experimental errors, the calculation errors of 4DOF model and 7DOF models were negligible under ideal conditions. The influence of frequency, amplitude, downstroke ratio on the inertial power and inertial force were plotted in Fig. 5. The results showed that, within the scope of the experimental and computational values, the inertial power, inertial lift and drag increased along with amplitude and frequency. Moreover, the inertial power, lift and drag decreased when going from low to medium downstroke ratios (0.35 to 0.55) and then increased slightly when downstroke ratio (0.55 to 0.65) increased further. Comparing the same 4DOF model of experiment and computation results, the computational power and force were smaller than the experimental values.

### 3.2. The inertial power and force on different coordinate axes

According to different flap amplitudes, the inertial power and force had obvious variations on three directions. Under different experiment conditions and for different bat species, the flap amplitudes of bats were also quite different. For the lesser dog-faced fruit bats (*Cynopterus brachyotis*) tested in the wind tunnel, the flap amplitudes were about 50° to 65° under lower to higher wind speed [22]. For the big brown bat (*Eptesicus fuscus*) in free flight, the flap amplitudes we got were across a range of 75° to 130°. The flap amplitude presented in the following model was 40°, 90°, 140° and 180°, these four characteristic values included the maximum values, minimum values and special values that adapted to all bat species.

For the simple sinusoidal flap motion of the 4DOF model, the variation tendencies of velocity, acceleration, inertial power and inertial force were studied. For the flap motion only, the variation tendency in a cycle of each arbitrary marker was the same as that of other separated or integrated markers. As there was no relative movements on the $X$ axis, the inertial power and force on $X$ direction were 0. Representative curves of wrist velocity, acceleration, inertial power and inertial force were presented in Fig. 6. The results indicated that when amplitude increased, the velocity, acceleration, inertial power and force on the $Y$ axis and $Z$ axis were also increased, but the increasing extent of these parameters on the $Y$ axis was higher. The cycles, positive peaks and negative peaks of $F_Z$ and $F_Y$ were highly related to the flap amplitude. At higher amplitudes, the curves of $P_Z$, $F_Y$ and $P_Y$ had relatively flat changes at the reversal position of upstroke and downstroke. In view of the normalized expressions, the resultant acceleration and force curves coincide. Therefore, only the resultant velocity, force and power curves were shown in Fig. 6. The cycle of these curves were twice of flap frequency. The resultant power and

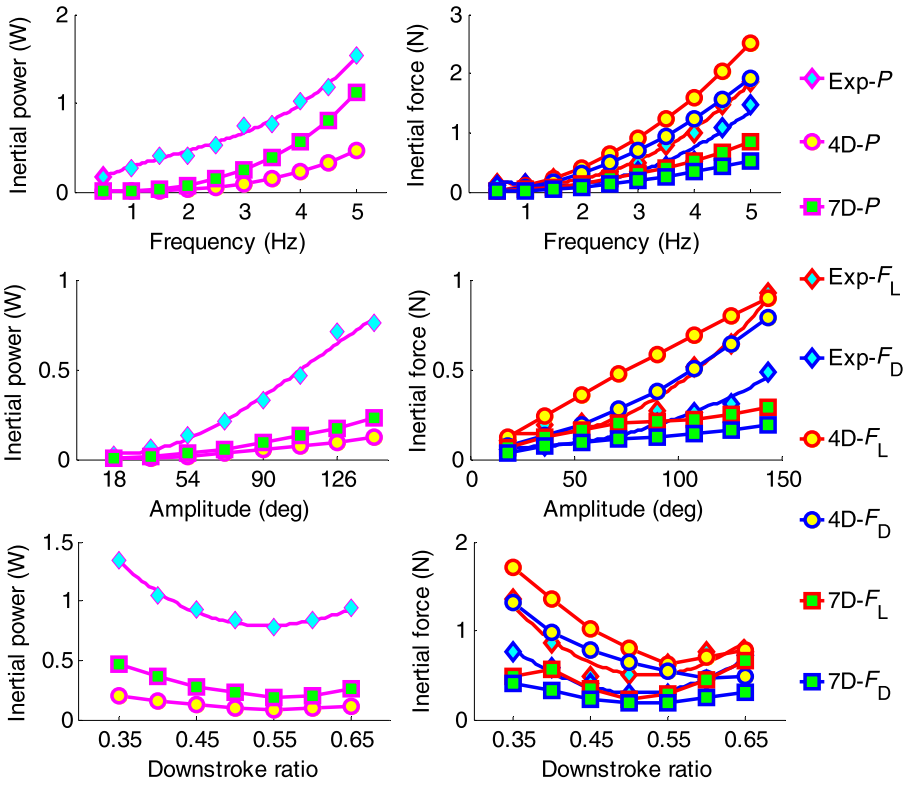


**Fig. 5.** The influence of frequency, amplitude, downstroke ratio on the inertial power and inertial force. Exp represent the experiment results of robotic bat wing, 4D, 7D respectively represent the calculation results of four degrees and seven degrees of freedom model. $P$, $F_L$, $F_D$ represent the inertial power, inertial force on lift direction and inertial force on drag direction. Note that, for the 7DOF model, the power data were magnified 100 times and the force data were magnified 10 times to compare the results in a graph.

velocity curves was similar to sine curves and the resultant force curves had a nearly reversal from small to large flap amplitude.

For the 7DOF model, the inertial power and force were also decomposed on three directions. According to different fragments, as each part has different mass, speed and acceleration properties, the inertial power and force were quite different from each other. Different from the flap motion only, the inertial power and force along the $X$ axis were no longer 0 under the combination of all motions (Fig. 7). The effects of humerus, radius and five digits on inertial power and force were studied separately. The results showed that the inertial power and force on the $X$ axis was larger than values on the $Z$ and $Y$ axis. The inertial cost on the $X$, $Y$ and $Z$ axes hold approximately 20%, 30% and 50% of the total power and the proportion of the inertial force on $X$, $Y$ and $Z$ axis was about 35%:25%:40%. For the energy expenditure and inertial forces, the radius accounted for the largest proportion, while the humerus and digit1 took the smallest proportions (Fig. 8).

## 4. Discussion

### *4.1. The effect of three parameters on inertial power and force*

The inertial power and force are related to the mass, velocity and acceleration. But, for a particular robotic bat wing, because of the constant density and size, the mass is unchangeable. When frequency, amplitude and downstroke ratio are compared together, because changing the downstroke ratios is made through varying the upstroke and downstroke frequencies in a cycle, this can also be attributed to the frequency factor [21]. So amplitude and frequency are two main and changeable factors that affect the inertial power and force. When the frequency increased, the flap time is decreased in one cycle and thus the velocity and acceleration are increased. Similarly, increasing the amplitude can increase the maximum flap distance and therefore promote velocity and acceleration likewise. From the theoretical equation (2), we find that the inertial power is proportional to the square of amplitude and the cubic of frequency, while the inertial force is proportional to amplitude and to the square of frequency. Compared with the results obtained with real bats, the theoretical and practical proportionality coefficient are slightly different [18]. One reason might due to that the theoretical motions are simplified to sinusoidal flap, but actually the motions of native bats are complicated. Another reason might be that when one parameter is studied, the changes in other parameters are not considered in our models. However, some parameters

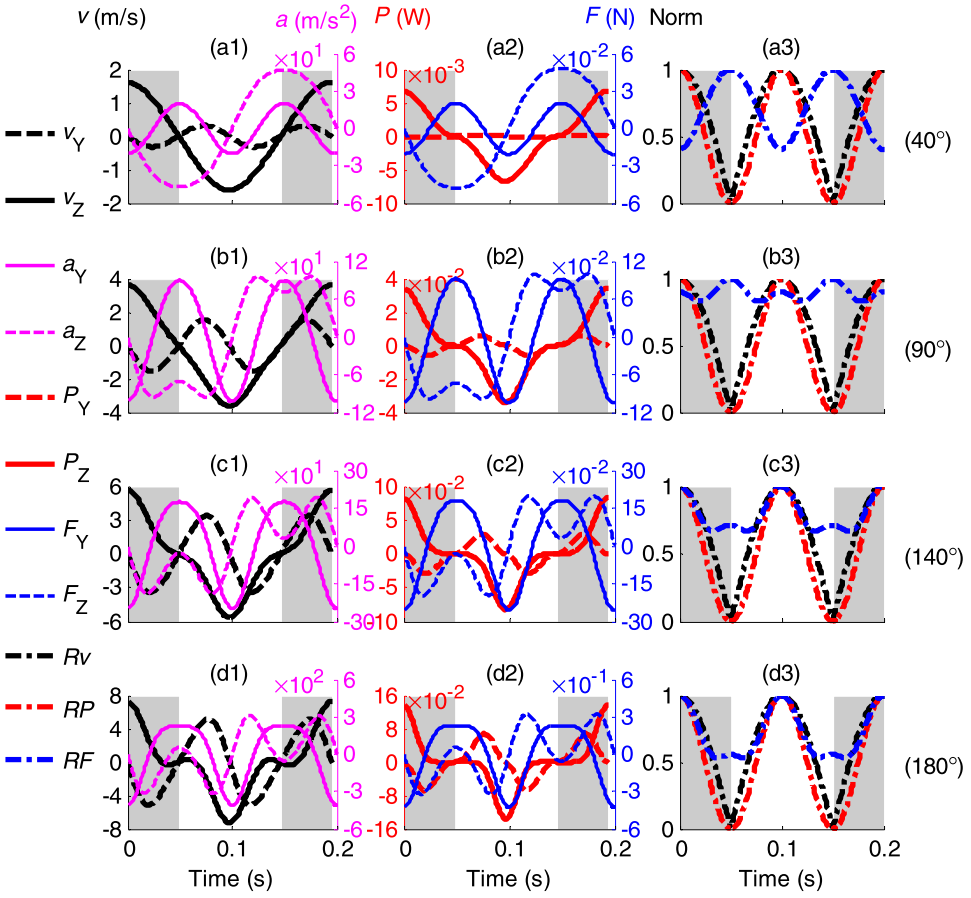


**Fig. 6.** The wrist joint velocity, acceleration, inertial power and force of the 4DOF model. $v_Y$, $v_Z$, $a_Y$, $a_Z$, $P_Y$, $P_Z$, $F_Y$, and $F_Z$ represent the wrist joint velocity on the $Y$ axis, the velocity on the $Z$ axis, the acceleration on the $Y$ axis, the acceleration on the $Z$ axis, the inertial power on the $Y$ axis, the inertial power on the $Z$ axis, the inertial force on the $Y$ axis, the inertial force on the $Z$ axis. *Rv*, *RP*, *RF* respectively represent the resultant velocity, resultant power and resultant force of the wrist joint. The flap amplitude of the first-row figures (a1, a2, a3), second-row figures (b1, b2, b3), third-row figures (c1, c2, c3) and fourth-row figures (d1, d2, d3) are 40°, 90°, 140°, 180° respectively. The left and right axis units of the first- and second-column figures are velocity (m/s), acceleration (m/s$^2$), inertial power (W), and inertial force (N), respectively. The axis units of the third column figures are normalized between 0 and 1 to compare velocity, power and force together. The gray backgrounds represent the downstroke period of a flap cycle.

will be changed simultaneously during bat flight [23], and each parameter has its upper and lower limits [4]. Such as the *Cynopterus brachyotis* flow in the wind tunnel, with wingbeat frequencies ranging between 7.6 Hz and 9.9 Hz, wingbeat amplitudes from 50° to 140° [2]. As it is difficult to establish precious theoretical equations on the inertial power and force of native bats, and the motions of robotic bat wings were often simplified to simple sinusoidal movements [11–15], the simple equations of flap flight still can provide some implications for robotic wing movements.

During the deceleration stage, the negative power will be generated (Fig. 6). However, our motors have no device to store the negative power. Even for the native bat, although some storage may occur late in upstroke, it does not appear to be large enough to account for the power loss [8]. So the wings of robotic bats should have a low inertia to minimize the inertial power requirements of flapping flight [17]. To decrease the inertial power or force for the future robotic bat wing, amplitude and frequency are two convertible characteristics needing to be reduced. Due to the scope of each factor, either of these parameters cannot be too big or small to reach the ideal values, but by properly controlling these two parameters, more efficient flight of the robotic bat wing can be achieved.

When the downstroke ratio deviated from the symmetric center ($\tau = 0.5$), it increases the upstroke or downstroke frequency and thus increased the maximum inertial power and force. For the symmetrical flap motion, the change trends should be standard symmetrical U-shaped curves. But our results showed that the effect of downstroke ratio to inertial power and force were not symmetrical U-shaped curves, and the values were a little smaller at higher downstroke ratio. These results indicated that at the same frequency, the inertial power and force of upstroke are smaller than downstroke. As the wings are mainly expanded at the downstroke but folded at the upstroke, this result verified that the biomimetic wing folding can reduce the inertial power and force [5].

For the same 4DOF model, the power and force of the computational values are smaller than the experimental results of robotic wing. The power differences may be due to the following reasons. One is that the experiment power is calculated

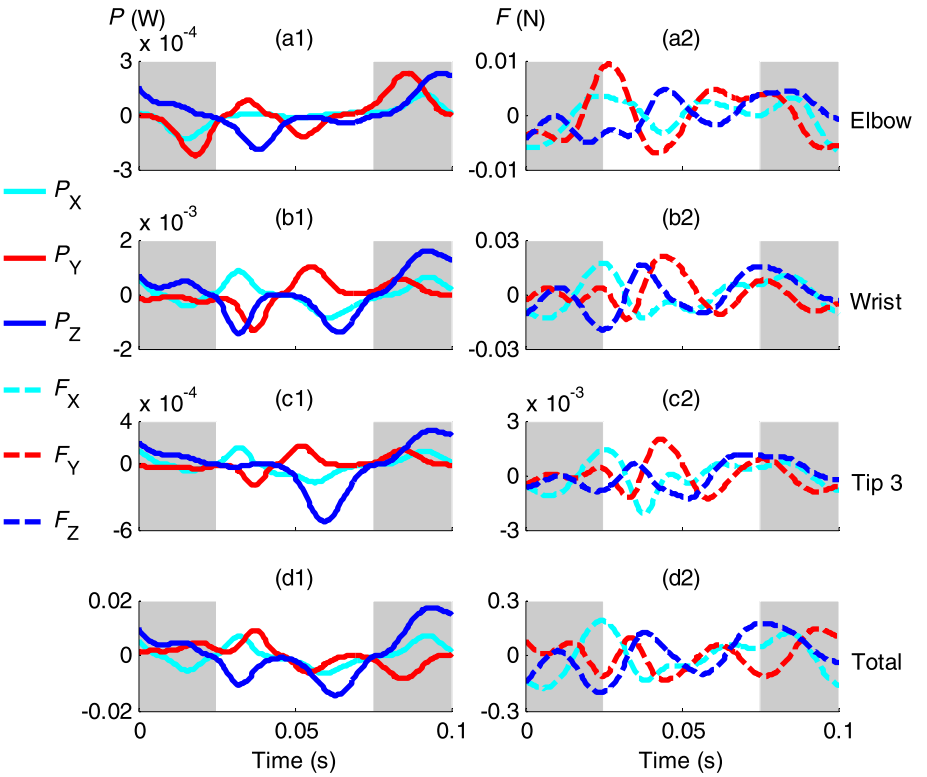


**Fig. 7.** The inertial power and force changing trends of different fragments. The fragments of a1 and a2, b1 and b2, c1 and c2, d1 and d2 are the elbow (r4) joint, the wrist (w1) joint, tip3 (d36) and the total skeletons respectively. The units of the first- and second-column figures are inertial power (W) and inertial force (N) respectively. The gray backgrounds represent the downstroke period of a flap cycle.

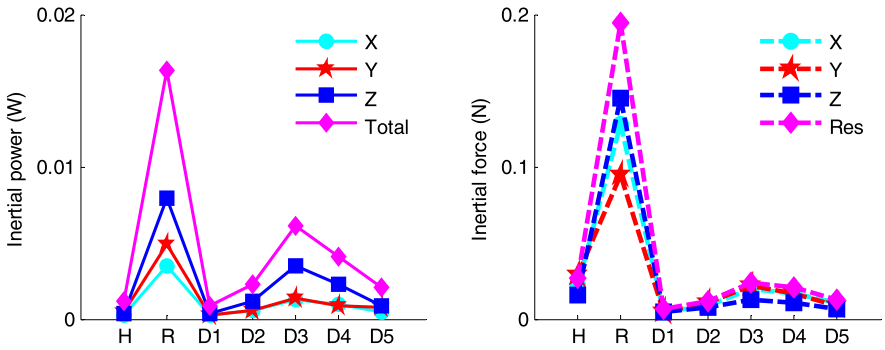


**Fig. 8.** The inertial power and force of different parts on three axes. H, R, D1, D2, D3, D4, D5 respectively represent humerus (h1–w1), radius (r1–r4), digit1 (d1), digit2 (d30–d23), digit3 (d31–d36), digit4 (d41–d46) and digit5 (d51–d56) part. $X$, $Y$, $Z$ represent the values on the $X$, $Y$, $Z$ axes. Total and Res represent the total power and the resultant forces on three axes.

as the energy cost of the motors, not the wing directly, and the motor efficiency is smaller than 1. The second is that the experimental wing is heavier as it contains the steel wire, metal pins or even small adhesive markers, which are neglected in the calculation model. The third is due to the frictions between different joints, and these are also not considered in calculation. The fourth is that the experimental results also contain the aerodynamic cost and aerodynamic force of the skeletons, although this effects are small. All these factors would make the experimental values larger than the results of theoretical calculations. The second to fourth reasons are also suitable for the explanation of the force differences.

### *4.2. The components of inertial power and force*

For the sinusoidal flap motion only, the flap angle $r(t)$ and velocity $\mathrm{d}r/\mathrm{d}t$ are presented in Eq. (1). The velocity components on horizontal axis ($v_Y$) and vertical axis ($v_Z$) can be calculated as follows

$$v_Y = \varphi\pi f \cos(2\pi ft) \times \sin\left(\frac{\varphi}{2}\cos(2\pi ft)\right)$$
$$v_Z = \varphi\pi f \cos(2\pi ft) \times \cos\left(\frac{\varphi}{2}\sin(2\pi ft)\right) \tag{5}$$

and the accelerations $(a_Y, a_Z)$ can be calculated as the derivative of the velocities $(v_Y,\ v_Z)$. So the curves and change trends in Fig. 6 can be formulated when different amplitudes $(\varphi)$ are substituted in the equations. For the flap motion, the calculation results demonstrated that the inertial power and force are related to the flap amplitude. At minor amplitude, the inertial power and force on the $Y$ axis $(P_Y, F_Y)$ are negligible. When amplitude increased, the increasing scope of inertial power and force on the $Y$ axis $(P_Y, F_Y)$ are larger than on the $Z$ axis $(P_Z, F_Z)$. These are mainly due to the fact that the growth rates of velocities and accelerations on the $Y$ axis are larger than that on the $Z$ axis. At the beginning and end of sinusoidal flap in a cycle, the changes in velocity and acceleration are slight, and these effects are more noticeable at higher amplitude, so some power and force curves had more or less flat trends according to the stroke reversals (Fig. 6). For the resultant power, the results were consistent with the conventional ratiocinations. The cycles of inertial power are twice as wing beat frequency, and with positive peaks during up-acceleration and down-acceleration stages, with negative peaks during up-deceleration and down-deceleration stages [15]. But the inertial forces are different, and no generic curve can be used to represent the changes at different amplitudes.

For the full motions, the inertial power and force still account for the largest part of the total value in the flap direction (Fig. 8). In comparison with the flap motion, the inertial power and force on the $X$ direction are no longer 0. The proportion of power and force on the $Z$ axis are decreased, but are increased on the $X$ and $Y$ axes. This implies that wing folding may decrease the inertial power and force on up–down direction but increase the values on expand–contract and back–forth direction. The increased force in the expand–contract direction means that more 'centripetal force' will be generated. For the robotic bat wing that uses flexible connection, such as scopes or wires, to connect skeletons and transfer motions, the sweep and elbow angles are not preciously constant during motions. The 'centripetal force' probably increases the angle differences from the set or required values. So when more degrees of freedom are added, measurements should be taken to avoid these problems.

In general, the fragments which are near the shoulder have relatively large masses, but have small velocities and accelerations, but it is exactly opposite when the fragments are far from the shoulder. The resultant values of the power and force depend on the interaction of these two factors. Although the mass of the radius are 22 times as the digit3 (Table 2), the inertial power and force of radius are roughly 2.7 and 8 times that of the digit3 (Fig. 8). Therefore, for the digit and other bones of the same mass, the digits need to bear larger forces. But digits are delicate and easy to break compared with other skeletons [13], so the stiffness of the digits should be strengthened in the design and fabrication of future robotic bat wings. Comparing the results in this paper with other literature data is difficult because the available data on the inertial power and force of native bat wing often include the power and force of the whole wing, including bat membrane [2,4,7]. The membrane occupies a large part of bat wing, and its effect on inertial power and force still needs to be further studied. Collecting accurate data on wing movements and membrane deformations are crucial for establishing a biomimetic bat wing model, and the inertial power and force of the whole bat wing can be estimated based on the new model.

**Acknowledgements**

The authors are thankful to professors Kenny Breuer and Sharon Swartz from Brown University for their knowledge about bat flight and for providing the wind-tunnel facility for the experiments. Furthermore, we thank Joe Bahlman, Cosima Schunk and Jean Baptiste for the robotic wing design and experiment. This work was supported by Joint Training Doctoral Project of China Scholarship Council, Southeast University (No. 3202003905) and Scientific Innovation Research of College Graduates in Jiangsu Province (No. CXLX12_0080).

## Appendix A

### *A.1. Theoretical derivations on flap movement of inertial power and force*

For a rigid wing, when the wing flaps with amplitude $\varphi$, the angular velocity $\omega$, the transient flap angle $r(t)$, the transient angular velocity $\mathrm{d}r/\mathrm{d}t$, and the transient angular acceleration $\mathrm{d}^2r/\mathrm{d}t^2$ can be described by the following equation

$$r(t) = \frac{1}{2}\varphi(\omega t) + \varphi_0$$
$$\frac{\mathrm{d}r}{\mathrm{d}t} = \frac{1}{2}\omega\varphi'(\omega t)$$
$$\frac{\mathrm{d}^2r}{\mathrm{d}t^2} = \frac{1}{2}\omega^2\varphi''(\omega t) \tag{6}$$

where $\varphi_0$ is the initial amplitude, the transient angular velocity, and the transient angular acceleration are the first- and second-order derivatives of the transient flap angle, respectively. The inertial energy $E$ of one wing can be calculated as the

product of the moment of inertia $I$, the angular velocity $\mathrm{d}r/\mathrm{d}t$, the angular acceleration $\mathrm{d}^2r/\mathrm{d}t^2$ and time $t$. The inertial energy through time can be modeled by the following integral equation:

$$E(t) = \int \left( I \times \frac{\mathrm{d}r}{\mathrm{d}t} \times \frac{\mathrm{d}^2 r}{\mathrm{d}t^2} \right) \mathrm{d}t = \frac{1}{4} \int I\omega^3 \varphi'(\omega t)\varphi''(\omega t)\mathrm{d}t = \frac{1}{8} I\omega^2 \left[\varphi'(\omega t)\right]^2 + C \tag{7}$$

where $C$ is the integration constant. The inertial power can be calculated as the product of inertial energy $E$ and frequency $f$. During one flap cycle, the wing has two acceleration and two deceleration phases, the acceleration inertial cost is the same as the deceleration inertial cost [7]. So the inertial power is four times that of each acceleration phase. To calculate the inertial power $P$, the positive increase in $E(t)$ over the course of one-fourth wingbeat cycle from $t = 0$ to $t = 1/(4f)$ is summed, the total inertial power is four times that period:

$$P = \int_0^{\frac{1}{4f}} f I\omega^3 \varphi'(\omega t)\varphi''(\omega t)\mathrm{d}t \tag{8}$$

based on the bat flap angle data (Fig. 1) and other simplified models to calculate the inertial power of a bird or a bat [7]; when small deviations are not considered, the flap motion can be simplified to a sinusoidal movement, the transient angle is given by

$$\varphi(\omega t) = \varphi \sin(2\pi f t) \tag{9}$$

Combining equations (6), (7), (8) and (9) gives the following equation (10) of the transient flap angle $r(t)$, the transient angular velocity $\mathrm{d}r/\mathrm{d}t$, and transient angular acceleration $\mathrm{d}^2r/\mathrm{d}t^2$.

$$\begin{aligned} r(t) &= \frac{1}{2}\varphi \sin(2\pi f t) + \varphi_0 \\ \frac{\mathrm{d}r}{\mathrm{d}t} &= \pi f \varphi \cos(2\pi f t) \\ \frac{\mathrm{d}^2 r}{\mathrm{d}t^2} &= -2\pi^2 f^2 \varphi \sin(2\pi f t) \end{aligned} \tag{10}$$

the inertial energy and inertial power of sinusoidal flap during a complete wingbeat cycle can be calculated as

$$\begin{aligned} E(t) &= \int \left( I \times \frac{\mathrm{d}r}{\mathrm{d}t} \times \frac{\mathrm{d}^2 r}{\mathrm{d}t^2} \right) \mathrm{d}t = -\int I\pi^3 f^3 \varphi^2 \sin(4\pi f t)\mathrm{d}t = \frac{1}{4} I\pi^2 f^2 \varphi^2 \cos(4\pi f t) + C \\ P &= -4 \int_0^{\frac{1}{4f}} I\pi^3 f^4 \varphi^2 \sin(4\pi f t)\mathrm{d}t = I\pi^2 f^3 \varphi^2 \end{aligned} \tag{11}$$

The values of $E(t)$ and $P$ are in accordance with D.K. Riskin's results [6], but half those of C. Vandenberg [7]. These differences lie in the different process methods to the negative power. The instantaneous inertial power is positive at the acceleration stage and negative at the deceleration stage. Whether the negative power can be stored and converted into useful aerodynamic work that occurs during wing deceleration was controversial, and these controversial results lead to a one to two times difference in the total power [6,7]. Unlike the native flight animals, the motor we used to measure the power has no device, such as elastic element to store the negative energy and convert to useful work during the acceleration stage. So only the positive work for two acceleration phases of one wing beat was considered, and the inertial power was calculated by product the positive work to the wing beat frequency. In accordance with the experimental settings, the negative power is also neglected in the following computational models. From the point of view of the variation tendency, while frequency, amplitude, and downstroke ratio to the inertial power and force were mainly studied in the present study, this assumption would not affect the variation pattern.

The inertial force $F$ can be calculated as the product of mass $m$ and linear acceleration $a$. The inertial force of the wing can be expressed as superposition of three orthogonal components values of the bat wing coordinate system. For each component, the linear displacement $s(t)$, the linear acceleration $\mathrm{d}^2s/\mathrm{d}t^2$ and the inertial force $F$ are given by

$$\begin{aligned} s(t) &= \frac{1}{2}x(\omega t) + x_0 \\ \frac{\mathrm{d}^2 s}{\mathrm{d}t^2} &= \frac{1}{2}\omega^2 x''(\omega t) \\ F &= \frac{1}{2} m\omega^2 x''(\omega t) \end{aligned} \tag{12}$$

where $x$ is the maximum displacement and $x_0$ is the initial displacement at each direction. Analogously, when the flap movement of a rigid wing skeleton is simplified to a simple harmonic motion, the linear displacement $s(t)$, the linear acceleration $\mathrm{d}^2s/\mathrm{d}t^2$ and the inertial force $F$ of each component can be expressed as:

$$\begin{aligned} s(t) &= \frac{1}{2}x\sin(2\pi ft) + x_0 \\ \frac{\mathrm{d}^2s}{\mathrm{d}t^2} &= -2\pi^2 f^2 x\sin(2\pi ft) \\ F &= -2m\pi^2 f^2 x\sin(2\pi ft) \end{aligned} \tag{13}$$

Note that, for any point of the rigid bat wing skeleton of flap motion, it moves in the up-down ($Z$) and stretch-contract ($Y$) directions. The inertial power and the inertial force are the superposition of these two components. In this respect, for the flap motion only, the wing has only two-dimensional motions in a plane. But when sweep, elbow, wrist and finger motions are considered, the wing has complex three-dimensional movements in space, and the above simplified models are not applicable in this case. To achieve accurate three-dimensional calculation, the bat wing skeleton was divided into some small parts. The inertial energy and inertial force were first calculated for each small part, and then accumulated to get the overall results of the bat wing skeleton. The inertial power is the sum of all positive changes in inertial energy over the course of the wingbeat cycle multiplied by the wingbeat frequency. The inertial energy $E$, the inertial power $P$ and inertial force $F$ of the bat wing skeleton are as follows:

$$\begin{aligned} E &= \frac{1}{2}\sum_{n=1}^{k} m_n v_n^2 \\ P &= Ef = \frac{1}{2}f\sum_{n=1}^{k} m_n v_n^2 \\ F &= ma = \sum_{n=1}^{k} m_n a_n \end{aligned} \tag{14}$$

where $n$ is the $n$th segment of the total separated part, $k$ is the total number of the small intersected part, $a$ is the synthetic acceleration and $v$ is the relative velocity of the segment to the shoulder.

### *A.2. The number of divided segments*

Some factors such as the number of skeleton divided parts may also affect the inertial power and force. To compare with the 35 fragments of the 4DOF model used in this paper, the fragments of the identical model were cut to 22 small fragments. With each 3 fragments at body, humerus, radius, digit3, digit4 and digit5 skeletons, and each 1 fragment at digit1, digit2, wrist joint and wrist-radius connect skeletons. The same strategy for these two models was used to calculate the inertial power and force, and the results indicated that the difference in inertial power between these two models was less than 3%. For the strip model results of native bat wing, the analysis indicated that when the number of strips was no less than 15, the 'doubled strip width error' was less than 3% [7]. This means that more divided parts cannot improve the accuracy of the calculation results.

## References

[1] J. Colorado, C. Rossi, A. Barrientos, D. Patino, The influence of bat wings for producing efficient net body forces in bio-inspired flapping robots, in: 2014 ICINCO, vol. 2, 2014, pp. 528–532.
[2] J. Iriarte-Diaz, D.K. Riskin, D.J. Willis, K.S. Breuer, S.M. Swartz, Whole-body kinematics of a fruit bat reveal the influence of wing inertia on body accelerations, J. Exp. Biol. 214 (2011) 1546–1553.
[3] H.M. Papadimitriou, S.M. Swartz, T.H. Kunz, Ontogenetic and anatomic variation in mineralization of the wing skeleton of the Mexican free-tailed bat, *Tadarida brasiliensis*, J. Zool. 240 (1996) 411–426.
[4] M. Thollesson, U.M. Norberg, Moments of inertia of bat wings and body, J. Exp. Biol. 158 (1991) 19–35.
[5] U.M. Norberg, T.H. Kunz, J.F. Steffensen, Y. Winter, O. Vonhelversen, The cost of hovering and forward flight in a nectar-feeding bat, *Glossophaga soricina*, estimated from aerodynamic theory, J. Exp. Biol. 182 (1993) 207–227.
[6] D.K. Riskin, A. Bergou, K.S. Breuer, S.M. Swartz, Upstroke wing flexion and the inertial cost of bat flight, Philos. Trans. R. Soc. Lond. B, Biol. Sci. 279 (2012) 2945–2950.
[7] C. Vandenberg, J.M.V. Rayner, The moment of inertia of bird wings and the inertial power requirement for flapping flight, J. Exp. Biol. 198 (1995) 1655–1664.
[8] T.L. Hedrick, J.R. Usherwood, A.A. Biewener, Wing inertia and whole-body acceleration: an analysis of instantaneous aerodynamic force production in cockatiels (*Nymphicus hollandicus*) flying across a range of speeds, J. Exp. Biol. 207 (2004) 1689–1702.
[9] T. Weis-Fogh, Energetics of hovering flight in hummingbirds and in Drosophila, J. Exp. Biol. 56 (1972) 79–104.
[10] U.M. Norberg, Aerodynamics, kinematics, and energetics of horizontal flapping flight in the long-eared bat *Plecotus auritus*, J. Exp. Biol. 65 (1976) 179–212.

[11] J. Colorado, A. Barrientos, C. Rossi, K.S. Breuer, Biomechanics of smart wings in a bat robot: morphing wings using SMA actuators, Bioinspir. & Biomim. 7 (2012) 036006.
[12] G. Koekkoek, F.T. Muijres, L.C. Johansson, M. Stuiver, B.W. van Oudheusden, A. Hedenstrom, Stroke plane angle controls leading edge vortex in a bat-inspired flapper, C. R., Méc. 340 (2012) 95–106.
[13] J.W. Bahlman, S.M. Swartz, K.S. Breuer, Design and characterization of a multi-articulated robotic bat wing, Bioinspir. & Biomim. 8 (2013) 016009.
[14] P. Chen, S. Joshi, S.M. Swartz, K.S. Breuer, J.W. Bahlman, G.W. Reich, Bat inspired flapping flight, SciTech AIAA paper 1120, 2014.
[15] J.W. Bahlman, S.M. Swartz, K.S. Breuer, How wing kinematics affect power requirements and aerodynamic force production in a robotic bat wing, Bioinspir. & Biomim. 9 (2014) 025008.
[16] A.R. Ennos, Inertial and aerodynamic torques on the wings of diptera in flight, J. Exp. Biol. 142 (1989) 87–95.
[17] S.C. Burgess, R.J. Lock, J. Wang, G.D. Sattler, J.D. Oliver, The effect of aerodynamic braking on the inertial power requirement of flapping flight: case study of a gull, Int. J. Micro Air Veh. 6 (2014) 117–127.
[18] X.D. Tian, J. Iriarte-Diaz, K. Middleton, R. Galvao, E. Israeli, A. Roemer, A. Sullivan, A. Song, S. Swartz, K. Breuer, Direct measurements of the kinematics and dynamics of bat flight, Bioinspir. & Biomim. 1 (2006) S10–S18.
[19] A.J. Bergou, S. Swartz, K. Breuer, G. Taubin, 3D reconstruction of bat flight kinematics from sparse multiple views, in: 2011 ICCV Workshops, IEEE, 2011, pp. 1618–1625.
[20] S.J. Agosta, Habitat use, diet and roost selection by the Big Brown Bat (*Eptesicus fuscus*) in North America: a case for conserving an abundant species, Mamm. Rev. 32 (2002) 179–198.
[21] R. von Busse, A. Hedenstrom, Y. Winter, L. Johansson, Kinematics and wing shape across flight speed in the bat, *Leptonycteris yerbabuenae*, Biol. Open 1 (2012) 1226–1238.
[22] T. Hubel, D. Riskin, S. Swartz, K. Breuer, Wake structure and wing kinematics: the flight of the lesser dog-faced fruit bat, *Cynopterus brachyotis*, J. Exp. Biol. 213 (2010) 3427–3440.
[23] U. Norberg, Y. Winter, Wing beat kinematics of a nectar-feeding bat, Glossophaga soricina, flying at different flight speeds and Strouhal numbers, J. 0Exp. Biol. 209 (2006) 3887–3897.